ACS Photonics

Open Access



pubs.acs.org/journal/apchd5

Article

# Low-Power Threshold Optical Bistability Enabled by Hydrodynamic Kerr Nonlinearity of Free Carriers in Heavily Doped Semiconductors

Huatian Hu,* Gonzalo Álvarez-Pérez, Tadele Orbula Otomalo, and Cristian Ciracì*

Cite This: *ACS Photonics* 2024, 11, 4812−4817

Read Online

ACCESS | Metrics & More | Article Recommendations | Supporting Information

**ABSTRACT:** We develop an efficient numerical model based on the semiclassical hydrodynamic theory for studying Kerr nonlinearity in degenerate electron systems such as heavily doped semiconductors. This model provides direct access to the electromagnetic responses of the quantum nature of the plasmons in heavily doped semiconductors with complex geometries, which is nontrivial for conventional frameworks. Using this model, we demonstrate nanoscale optical bistability at an exceptionally low-power threshold of 1 mW by leveraging Kerr-type hydrodynamic nonlinearities supported by the heavily doped semiconductor's free carriers. This high nonlinearity is enabled by a strong coupling between metallic gap plasmons and longitudinal bulk plasmons in the semiconductor due to quantum pressure. These findings offer a viable approach to studying Kerr-type nonlinearity and lay the groundwork for developing efficient and ultrafast all-optical nonlinear devices.

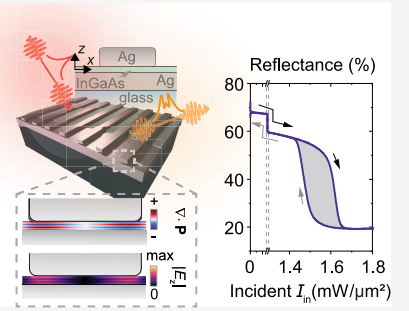


**KEYWORDS:** *plasmonics, nonlinear optics, semiconductors, optical Kerr effect, hydrodynamic theory, time domain, longitudinal modes*



## INTRODUCTION

The optical Kerr effect is a third-order nonlinear phenomenon that allows modulating the refractive index of the materials according to the applied electric field intensity.[1] Exploiting such an effect to attain efficient and ultrafast photon−photon interactions has long been sought after for the potential applications in all-optical information processing and storage.[2−10] More recently, the advent of artificial intelligence has led to an exponential increase in the demand for low-power computation solutions, bringing renewed interest in integrated all-optical nonlinear systems.

Semiconductors represent in this context an interesting class of materials, as they are compatible with large-scale fabrication methods for integrated devices while also supporting some of the largest optical nonlinearities.[11,12] When heavily doped, semiconductors can undergo a transition from the quantum regime, where their response is governed by single-particle excitations, to the classical regime of collective plasmon oscillations.[12] Due to the hydrodynamic nature of nonequilibrium carriers, collective plasmons can exhibit an intrinsic and strong free carrier optical nonlinearity.[2,13−17] Although these properties occur, in principle, in all degenerate electron systems, they are significantly larger for materials with low equilibrium density and small effective mass, such as doped InP and InGaAs.[18] In fact, very recently, it has been experimentally shown by measuring third-harmonic generation from heavily doped InGaAs nanoantennas that free electron nonlinearities can easily overcome intrinsic $\chi^{(3)}$ nonlinearities.[19] The drawback, however, is that free electrons inside a material mostly respond to external optical fields that oscillate below the plasma frequency as surface plasmons. This confines hydrodynamic nonlinear interactions at the material surface,[13,14,17] severely limiting the Kerr effect.

In this context, longitudinal bulk plasmons (LBPs) − charge density waves occurring in the *bulk* of spatially dispersive materials[20−22] − become very relevant. The relative distribution of the electrons over a positively charged background generates their characteristic longitudinal electric fields.[23] LBPs have been observed in thin metal films where they naturally occur in the ultraviolet energy range.[24,25] More recently, LBP resonances have been observed in transparent conducting oxide materials in the infrared, such as doped cadmium oxide.[26] Existing above the plasma frequency, the LBP sacrifices the typical field confinement associated with surface plasmons for a much larger active volume for nonlinear interactions, unlocking a new mechanism for low-power Kerr nonlinearity at the nanoscale.

From a theoretical perspective, LBP modes can be excited in finite size systems only if the response of the material is *nonlocal*.[21,27] One way to account for nonlocality in degenerate electron systems is to model the classical free electron dynamics incorporated with density-dependent energy potentials that encapsulate their quantum properties. This approach

**Received:** July 17, 2024
**Revised:** September 12, 2024
**Accepted:** September 12, 2024
**Published:** September 19, 2024

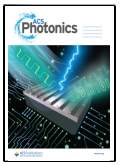





https://doi.org/10.1021/acsphotonics.4c01308
*ACS Photonics* 2024, 11, 4812−4817

is usually referred to as *hydrodynamic theory* (HT).[28,29] For a proper choice of the kinetic energy potential, it can be shown that the HT is equivalent to the Schrödinger equation for single-particle systems (or more precisely, single orbital systems).[30] Interestingly, the HT maintains its *quantum* structure for systems characterized by many electrons, as long as they can be considered as a collective quasiparticle, such as plasmons. With this premise, quantum size resonances, especially the intersubband transition plasmons, in quantum-confined systems (i.e., quantum wells) in traditional semiconductors can be seen from a theoretical point of view as equivalent to quantized LBP modes. Quantum well states have been indeed experimentally observed in metals.[31−33] The coupling between semiconductor quantum wells intersubband transitions and photonic systems has been experimentally exploited for linear[34,35] and nonlinear[11,32,33,36] optical modulations. However, modeling such collective intersubband plasmon oscillations in the conduction band of the quantum wells coupled with complex photonic structures typically relies on the combination of separate steps: calculate the band information with effective parameters derived and predict optical responses with separate semiclassical or phenomenological models such as coupled mode theory.[37,38]

In contrast, in this paper, we develop an ad hoc time-domain electromagnetic model integrated with semiclassical HT that can directly access the linear and nonlinear optical responses arising from the quantum nature of electrons, which is typically nontrivial for conventional semiconductor frameworks based on Schrödinger-Poisson equations.[31,32,39] With this model, we consider for the first time the plasmonic hydrodynamic contributions to Kerr nonlinearity in heavily doped semiconductors and demonstrate that LBP strongly coupled with gap surface plasmons can indeed drive a very large Kerr effect with a wide hysteresis in subwavelength volumes. As a result, an ultralow threshold (~1.55 mW/$\mu$m$^2$) and compact optically bistable device is proposed.

## RESULTS AND DISCUSSION

The many-body nature of a free electron gas driven by electromagnetic fields $\mathbf{E}(\mathbf{r}, t)$ and $\mathbf{H}(\mathbf{r}, t)$ can be described, within the HT, through two macroscopic fields, the electron density $n(\mathbf{r}, t)$ and velocity $\mathbf{v}(\mathbf{r}, t)$:

$$m_e\left(\frac{\partial}{\partial t} + \mathbf{v}\cdot\nabla + \gamma\right)\mathbf{v} = -e\left(\mathbf{E} + \mathbf{v}\times\mu_0\mathbf{H}\right) - \nabla\frac{\delta G[n]}{\delta n} \tag{1}$$

with $m_e$ and $e$ being the effective electron mass and the electron charge, respectively; $\gamma$ is the phenomenological damping rate; and $\mu_0$ is the vacuum permeability. The terms from left to right in eq 1 account for time evolution, convection, dissipation, Coulomb, Lorentz, and internal energy potential, i.e., quantum pressure, respectively. Since we are not interested in electron spill-out effects, here, we consider the energy functional within the Thomas−Fermi (TF) approximation $G[n] \simeq T_{TF}[n]$.[28] Introducing the polarization field defined as $\partial\mathbf{P}/\partial t = \mathbf{J} = -en\mathbf{v}$, expanding the nonlinear terms up to the third order and neglecting the higher-order nonlinear terms,[16] we obtain the following equation (see Supporting Information for detailed derivation):

$$\frac{\partial^2\mathbf{P}}{\partial t^2} + \gamma\frac{\partial\mathbf{P}}{\partial t} = \frac{n_0e^2}{m_e}\mathbf{E} + \beta^2\nabla(\nabla\cdot\mathbf{P}) + \mathbf{S}^{NL} \tag{2}$$

where the first-order quantum pressure term has been written as $\nabla\left(\frac{\delta T_{TF}}{\delta n}\right)_1 = \frac{m_e}{en_0}\beta^2\nabla\left(\nabla\cdot\mathbf{P}\right)$, where the parameter $\beta$ is related to the speed of sound in the Fermi-degenerate plasma $v_F$, $\beta^2 = \frac{1}{3}v_F^2 = \frac{10}{9}\frac{c_{TF}}{m_e}n_0^{2/3}$, $c_{TF} = \frac{\hbar}{m_e^2}\frac{3}{10}(3\pi^2)^{2/3}$. All of the higher-order terms containing the nonlinear responses to the external field and electron−electron interactions are encapsulated into the total nonlinear source $\mathbf{S}^{NL}$, which will be elaborated on later in eq 4a and 4b. Its origin should not be confused with the bulk nonlinear susceptibility $\chi^{(3)}$ that comes from the anharmonic potential experienced by the electrons in the crystals. The former is mostly a nonlocal response depending on the gradient of the fields, and the latter is a local response that will be considered separately in the wave equation as eq 5.

Let us start with the simplest system supporting quantized LBP modes (hereafter, we directly use LBP to refer to this *quantized* LBP resonance for simplicity): a thin slab excited by *p*-polarized light at oblique incidence of $\theta = 60°$, as depicted in Figure 1a. Note that *s*-polarized light cannot excite the LBP.

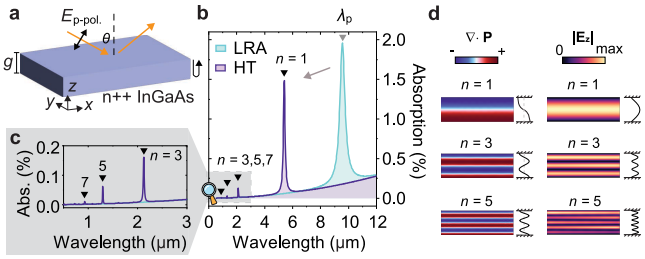


**Figure 1.** Optical absorption of a heavily doped InGaAs thin slab. (a) Schematic. (b) Linear absorption spectra of the thin slab with a local response approximation model (LRA, cyan) and nonlocal hydrodynamic theory (HT, purple). (c) Zoom-in plot of the higher-order LBPs. (d) Induced charge $\nabla\cdot\mathbf{P}$ and electric field of LBPs with an order of $n$ = 1, 3, 5.

An electric field with a nonzero normal component at the material interface is required to align with the charge oscillations necessary for driving LBP. The linear properties of LBP can be obtained in the frequency domain by solving the linear part of eq 2 (i.e., $\mathbf{S}^{NL} = 0$) coupled to the wave equation:

$$\nabla\times\nabla\times\mathbf{E} - \varepsilon_r\frac{\omega^2}{c^2}\mathbf{E} - \mu_0\omega^2\mathbf{P} = 0 \tag{3}$$

where $\varepsilon_r$ is the relative permittivity accounting for the dielectric local response and $c$ is the speed of light in vacuum.

We consider a thin layer ($g$ = 10 nm) of heavily doped InGaAs with equilibrium carrier density $n_0 = 6\times10^{18}$ cm$^{-3}$. The doped InGaAs can be described as a Drude-like material with $\varepsilon_{inf} = 12$, $\gamma = 8.9$ ps$^{-1}$, and $m_e = 0.041m_0$ ($m_0$ being the electron mass). The parameters were taken by fitting the experimental data in ref 19 such that the screened bulk plasma wavelength lays at $\lambda_p = 2\pi c\sqrt{(m_e\varepsilon_0\varepsilon_{inf}/(n_0e^2))} = 9.56\ \mu$m.

The linear absorption spectra with and without quantum pressure are shown in Figure 1b,c. With local response approximation (LRA), a prominent absorption peak arises due to the epsilon-near-zero (ENZ) enhancement at $\lambda_p$. However, as electron−electron interactions are considered with the HT, the ENZ resonance exhibits a noticeable blueshift, accompanied by the emergence of additional higher-order resonances fulfilling the LBP condition of $\varepsilon(\omega, \mathbf{k}) = 0$. Only LBP modes


https://doi.org/10.1021/acsphotonics.4c01308
ACS Photonics 2024, 11, 4812−4817

with odd orders ($n$ = 1, 3, 5, ⋯) have a net dipole moment that can be excited by a plane wave. In Figure 1d, the charge density and electric field distributions clearly show the nodes and antinodes of the standing waves formed by the charge density oscillations. The energy and the intensity of these quantized modes greatly depend on the thickness of the slab due to the confinement in that dimension, similar to quantum wells.

Although appreciable, LBP modes in a thin slab display an absorption, in the best case, of only ∼1.5% (similar values are observed for the reflectance). Higher-order resonances, shown in Figure 1c, have even smaller absorption peaks (less than 0.2%). This is not surprising since the LBPs can couple only weakly to the transverse plane wave in free space. This characteristic hinders both the experimental observation and the application in linear and nonlinear devices.

To overcome this issue, we consider a hybrid system constituted by a thin layer of heavily doped InGaAs sandwiched between a silver film and an array of silver stripes (Figure 2a), which is experimentally feasible.[36,38] Such systems

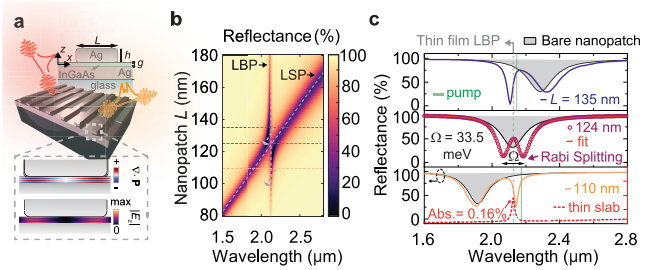


**Figure 2.** Hybrid bulk-plasmon slab-nanopatch system. (a) Schematic of the hybrid structure; height $h$ and periodicity $P_x$ of the antenna are 50 and 200 nm, respectively. Length, $L$, can vary. Bottom panels: the induced charges and electric field of the LBP in the thin spacer. (b) Strong coupling between LSP and LBP with a clear Rabi splitting in reflectance spectra, where three particular cases of different $L$ marked by dashed lines are shown in (c) for details. Gray shades in (c) represent the reflectance of the bare nanopatch without nonlocality. Reflectance spectrum of the on-resonance case ($L$ = 124 nm) is fitted with a Rabi splitting of Ω = 33.5 meV. Green shades mark the center wavelengths of the pump for probing Kerr nonlinearities.

are usually referred to as nanopatch antennas, in analogy to their radio frequency homologue. Nanopatch antennas have an absorption cross-section that is much larger than their physical dimensions and can concentrate far-field radiation into deep subwavelength nanogaps.[40] Additionally, the strong nanogap normal fields ($\mathbf{E}_z$) are perfectly aligned with the longitudinal fields of the LBP supported by the semiconductor film (lower panel in Figure 2a).

The hybrid structure is designed as follows: Since the LBP is mostly determined by the thickness and doping of the InGaAs, we fix $g$ and $n_0$ as the same as those described in Figure 1 such that the third-order LBP resonance is within the range of the nanopatch fundamental mode, i.e., ∼2.15 $\mu$m, as shown in Figure 2b. By adjusting the length $L$ of the nanopatch antenna, we can tune the resonances of the antenna localized surface plasmon (LSP) and its spectral overlap with the LBP. Because of the relatively large size and high equilibrium electron density of the silver nanopatches, the nonlocality and free electron nonlinearity can be negligible. In Supporting Information S3, we also apply hydrodynamic theory to silver for validation. Thus, we treat silver as a local Drude metal with $\varepsilon_{inf}$ = 4.039, $\omega_p$ = 9.172 eV, and $\gamma$ = 0.0207 eV.[41]

The detuning between the LBP and the LSP is an essential factor for the coupling. In Figure 2b, we map the reflectance of the system as a function of the incident wavelength and nanopatch $L$, which highlights the anticrossing dispersion between the LBP and LSP. The map shows antipeaks down to virtually zero reflectance, unveiling a nearly perfect absorption behavior.[42] Even when the two modes are quite detuned (e.g., $L$ = 140 nm), the absorption (81.7%) of the LBP is still enormously enhanced compared to the bare InGaAs slabs (0.16% in Figure 1c). This is due to the broad line width of the LSP resonances of the nanopatch, which can still provide decent field enhancements at certain detunings. This is substantial as the hybrid mode provides a practical and efficient way to access the elusive LBP in the previous experiment.[26]

When the two uncoupled states perfectly overlap, i.e., for $L$ = 124 nm, they hybridize into two modes with identical line width. By fitting the Rabi splitting with a temporal coupled mode theory,[43] it is possible to confirm that the system is working in a strong coupling regime. We have found that the relation between the coupling strength $g_c$ (contributing to Rabi splitting Ω = $2g_c$ = 33.5 meV) and the sum of half-width at half-maximum of each bare mode $\Sigma_i(\Gamma_i/2)$ satisfies the well-known condition $4g_c/\Sigma_i(\Gamma_i) = 1.26 > 1$, which indicates by a large margin that the system is indeed working in the strong coupling regime. As a consequence, the two resulting dressed states (i.e., the two peaks in the spectra) are hybrid bulk-surface plasmons. These hybrid modes hold the potential to inherit both the strong field enhancement from the LSP and the strong free electron nonlinearity from the LBP, providing a promising direction for the development of efficient and low-threshold nonlinear devices.

To prove this, let us investigate the hydrodynamic Kerr nonlinearity supported by the dressed LBP state in the hybrid system. The free carrier Kerr-type nonlinearity in the doped semiconductor is assumed to mainly come from the third-order hydrodynamic contributions in the constitutive relation eq 2, which arise from the convection and TF pressure, i.e., $\mathbf{S}^{NL} = \mathbf{S}^{cv} + \mathbf{S}^{TF}$, where (see Supporting Information for derivations):

$$\begin{aligned}\mathbf{S}^{cv} = &-\frac{1}{e^2 n_0^2}[(\nabla\cdot\mathbf{P})\dot{\mathbf{P}}(\nabla\cdot\dot{\mathbf{P}}^*) + (\nabla\cdot\mathbf{P})\dot{\mathbf{P}}^*(\nabla\cdot\dot{\mathbf{P}}) \\ &+ (\nabla\cdot\mathbf{P}^*)\dot{\mathbf{P}}(\nabla\cdot\dot{\mathbf{P}}) + (\nabla\cdot\mathbf{P})\dot{\mathbf{P}}\cdot\nabla\dot{\mathbf{P}}^* \\ &+(\nabla\cdot\mathbf{P})\dot{\mathbf{P}}^*\cdot\nabla\dot{\mathbf{P}} + (\nabla\cdot\mathbf{P}^*)\dot{\mathbf{P}}\cdot\nabla\dot{\mathbf{P}} + \dot{\mathbf{P}}\cdot\dot{\mathbf{P}}\nabla(\nabla\cdot\mathbf{P}^*) \\ &+ 2\dot{\mathbf{P}}\cdot\dot{\mathbf{P}}^*\nabla(\nabla\cdot\mathbf{P})]\end{aligned} \tag{4a}$$

$$\mathbf{S}^{TF} = -\frac{1}{9}\frac{\beta^2}{e^2 n_0^2}\nabla[(\nabla\cdot\mathbf{P})^2(\nabla\cdot\mathbf{P}^*)] \tag{4b}$$

The "·" over the variables denotes the time derivative, while the "*" denotes the complex conjugated. Note that because $\mathbf{S}^{NL} \propto 1/n_0^2$, these nonlinear terms, usually neglected in noble metals, become significant in semiconductors.[18] In our calculation, the equilibrium density $n_0$ in heavily doped InGaAs is nearly 4 orders of magnitude less than that of noble metals, enhancing nonlinear sources by 8 orders of magnitude.


https://doi.org/10.1021/acsphotonics.4c01308
ACS Photonics 2024, 11, 4812−4817

Equations 2 and 4a are solved with the wave equation for the magnetic vector potential $\mathbf{A}(\mathbf{r}, t)$:

$$\nabla \times \nabla \times \mathbf{A} + \frac{\varepsilon_r}{c^2}\frac{\partial^2 \mathbf{A}}{\partial t^2} + \mu_0 \frac{\partial}{\partial t}(\mathbf{P} + \mathbf{P}_d^{NL}) = 0 \quad (5)$$

The vector potential $\mathbf{A}$ works in the Coulomb gauge with a vanishing gradient of the scalar potential due to the absence of a static field such that the electric field $\mathbf{E} = -\partial\mathbf{A}/\partial t$ and magnetic field $\mu_0\ \mathbf{H} = \nabla \times \mathbf{A}$. The linear and nonlinear hydrodynamic contributions are coupled into the wave equation through a polarization vector $\mathbf{P}$. The lattice Kerr nonlinearity from the dielectric $\chi^{(3)} = 1.6 \times 10^{-18}\ m^2/V^2$ is considered through another polarization term $\mathbf{P}_d^{NL} = 3\varepsilon_0\chi^{(3)}|\mathbf{E}|^2\mathbf{E}$.[1] The contributions from the free carriers (i.e., $\mathbf{S}^{NL}$) and dielectric $\chi^{(3)}$ (i.e., $\mathbf{P}_d^{NL}$) will be separated and compared. Other nonlinear contributions including higher-order and cascaded processes are beyond the scope of this letter and have been excluded from consideration.

The system of eqs 2, 4a, 4b, and 5 is solved with a finite element method in the time domain through a customized implementation carried out using COMSOL Multiphysics. The driving field is continuous, and the incident intensity is gradually increased and decreased (will be discussed as Figure 3c) to adiabatically sweep out the nonlinear reflectance and

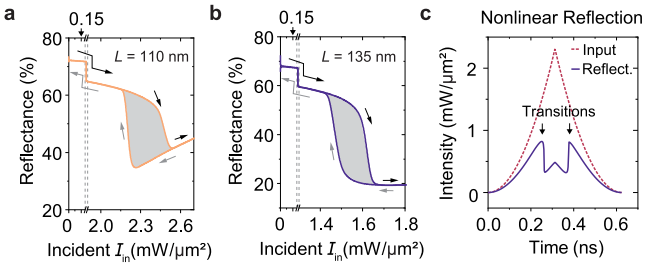


**Figure 3.** Hysteresis loop of two-dimensional nonlinear nanopatch systems. Prominent optical bistabilities with two particular antenna sizes: (a) $L$ = 110 nm and (b) $L$ = 135 nm. (c) Nonlinear reflection (pulse distortion) due to the bistability with $L$ = 135 nm.

hysteresis loop. Also, see video in Supporting Information for the probing scheme. To improve the computational efficiency and reduce the cost, we have implemented a time domain pulse envelope method in which the fast time-varying components from the full time-evolving field are separated, i.e., all the fields are expressed as $\mathbf{F}(\mathbf{r}, t) = \tilde{\mathbf{F}}(\mathbf{r}, t)e^{-i\mathbf{k}\cdot\mathbf{r}+i\omega t}$, with $\mathbf{F} = \mathbf{E}, \mathbf{H}, \mathbf{P}, \mathbf{A}$. Here, $\mathbf{k}$ and $\omega$ are the carrier wave vector and frequency, respectively, of the initial field. The tilde indicates the corresponding slowly varying envelope field. Solving for the envelopes allows for a much larger time step (e.g., $\sim 10^2$ times the wave period). To take into account the transformation above, all of the equations must be modified assuming the following transformations: $\nabla \rightarrow \nabla - i\mathbf{k}$ and $\partial/\partial t \rightarrow \partial/\partial t + i\omega$. In our calculations, we neglect the hydrodynamic nonlinear contribution from silver due to its high equilibrium charge density, which leads to a negligible nonlinear contribution.[16] To verify this, we also consider the hydrodynamic contributions from silver in Supporting Information S3; however, this does not result in any significant improvement. This is due to the hydrodynamic contributions in the nonlinear source from InGaAs being much stronger than those from silver (Supporting Information Figure S2c).

To understand the role played by the LBP-LSP coupling in the nonlinear process, we now study in detail three specific detuning situations, as summarized in Figure 2c. As the LBP is red-detuned from the LSP ($L$ = 110 nm, bottom panel of Figure 2c), we use the sharp resonance at 2.142 $\mu$m for achieving optical bistability. We set the input signal carrier wavelength slightly above the resonance, at 2.165 $\mu$m, to probe the hysteresis loop. As a result, with the increase of pumping power, the Kerr nonlinearity will shift the resonance toward lower energies so that the resonance will gradually overlap with the pump frequency. As shown by the guide-to-eyes gray arrow in Figure 2b for $L$ = 110 nm (orange line), the reflectance would see a decrease until it crosses the dip and then experiences an increase again.

By modulating the input intensity, we can generate the full hysteresis loop shown in Figure 3a, whose reflectance has bistable states with "on" and "off" states between ~60% and 30% with a threshold starting around 2.45 mW/$\mu$m$^2$. This situation could have a higher reflectance at the starting point, but the red-detuned LBP tends to move away from LSP which degrades the low reflectance dip. Likewise, we could switch off the hydrodynamic nonlinear sources ($\mathbf{S}^{NL} = 0$) and study the responses solely from enhanced dielectric nonlinearity $\mathbf{P}_d^{NL}$. The results show no bistability, confirming that the hydrodynamic Kerr nonlinearity is dominating (Supporting Information Figure S1a). In addition, we keep increasing the incident intensity to allow dielectric $\mathbf{P}_d^{NL}$ to trigger the nonlinearity. As shown in Supporting Information Figure S1b, the threshold intensity is 5 orders of magnitude higher than that with hydrodynamic Kerr effect. In addition, the hysteresis window becomes extremely narrow compared with Figure 3a. It means that the combination of the narrow line width and the strong hydrodynamic Kerr effect is the key to the low-threshold wide hysteresis loop.

While the situation in which the LBP and LSP resonances are overlapped (Figure 2c, with $L$ = 124 nm) is interesting from a linear response point of view, it does not represent a viable starting point for carrying out bistability since the LBP sharp resonance is hybridized and hence broadened. This results in a higher intensity threshold and a narrower hysteresis loop.

Let us now consider the opposite situation where the LBP is blue-detuned from the LSP, taking $L$ = 135 nm for instance, and tuning the pumping wavelength at 2.135 $\mu$m. Instead of getting away from the LSP, the LBP is now pushed by the nonlinearity toward the LSP, as shown by the guide-to-eyes gray arrow in Figure 2b for $L$ = 135 nm (purple line). The reflectance will decrease and cross the dip, instead of increasing as in the previous situation, due to the broadening of the branch in Rabi splitting. This causes a "flat" off-state in Figure 3b with a 20% reflectance. We can interpret this result as a self-modulated dynamic transition from detuned coupling to resonant strong coupling driven by the nonlocal Kerr nonlinearity. Moreover, the LBP is moving toward the LSP to gradually get a larger field enhancement and greater coupling due to the spectra overlap. This further lowers the intensity threshold for achieving optical bistability: 1.55 mW/$\mu$m$^2$ for achieving 70% to 20% branches with 5.4 dB modulation depth, inferring the effectiveness. As shown in Supporting Information Figure S3, this low-intensity threshold can remain robust even when accounting for increased damping $\gamma$, which may come from fabrication imperfections or other factors in the experiment. The threshold is maintained


https://doi.org/10.1021/acsphotonics.4c01308
ACS Photonics 2024, 11, 4812−4817

at a level of 10 mW/$\mu$m$^2$ as the damping grows to 30 ps$^{-1}$. Even as damping becomes very large ($\gamma$ = 40 ps$^{-1}$) such that the LBP modes become weak and flat (Figure S3a), a sigmoid-function-like nonlinear response can still be expected at a level of 10 mW/$\mu$m$^2$. Besides, the dielectric $\chi^{(3)}$ contribution is again negligible compared with the hydrodynamic ones (Supporting Information Figure S1), revealing the advantage of the free carriers as a nonlinear source for the Kerr effect.

In Figure 3c, we depict the nonlinear reflection against the input light (red dash line). We can observe that the reflected signal is dramatically distorted due to the transitions at a threshold intensity. Other thermal and nonthermal nonlinearity might be considered separately especially when the system is excited by an ultrashort pulse with strong peak intensity.[5,44] These are not considered in the current work because the scope of the present work focuses on the hydrodynamic contributions in Kerr nonlinearity with a much lower excitation intensity. Although this threshold is comparable to previously considered systems,[3,4,7,45,46,47] the required intensity could be further reduced to ~$\mu$W/$\mu$m$^2$ if one can overcome the high computational cost and consider a full three-dimensional nanopatch antenna system, which would provide an extra enhancement due to the additional transverse confinement. More interestingly, applying a bias voltage to the semiconductors through the metal patches on top can be expected to allow for the active control of the Kerr nonlinearity due to the charge depletion. Potentially, 1−2 orders of the magnitude drop of the threshold can be expected.[17] Furthermore, the switching time, which determines the limit of the operation frequency, is another important factor. In Supporting Information Figure S4, we simulate the optical switching response of the structure. The switching-on and -off times can be approximately 1 ps. (see detailed discussion in Supporting Information S5). Overall, this low-power threshold enables an efficient switch between two states, while the decent modulation depth ensures the effectiveness and fidelity of the modulation process. Our finding of high hydrodynamic Kerr nonlinearity could enable crucial applications in optical data processing, such as memory, binary switching, and logic functions.

## CONCLUSIONS

In conclusion, we proposed an ad hoc numerical approach based on the finite element method in the time domain to self-consistently solve intensity-dependent equations at the nanoscale. By selecting appropriate kinetic energies and quantum potentials in the semiclassical HT, this approach is able to describe the behaviors of the quantized resonances in degenerate electron systems, including the intriguing nonlinearities from the intersubband transitions. More importantly, by leveraging the strong coupling between LBP and LSP, we explored the impact of the hydrodynamic Kerr nonlinearity and demonstrated large contrast bistability with a power threshold of ~1 mW (considering a full patch and a focused beam area to the diffraction limit). Our findings open a viable avenue for studying and designing ultrafast all-optical integrated circuits.

## ASSOCIATED CONTENT

### Supporting Information

The Supporting Information is available free of charge at https://pubs.acs.org/doi/10.1021/acsphotonics.4c01308.

Derivation and implementation method of hydrodynamic nonlinear sources and contributions from dielectric $\chi^{(3)}$ in the nonlinear reflectance, hydrodynamic contributions from silver and heavily doped InGaAs, robustness of the system with different dampings, and switching time (PDF)

Video of temporal evolution of the nonlinear system (MP4)

## AUTHOR INFORMATION


### Corresponding Authors

**Huatian Hu** − *Istituto Italiano di Tecnologia, Center for Biomolecular Nanotechnologies, 73010 Arnesano, Italy;* orcid.org/0000-0001-8284-9494; Email: huatian.hu@iit.it

**Cristian Ciracì** − *Istituto Italiano di Tecnologia, Center for Biomolecular Nanotechnologies, 73010 Arnesano, Italy;* orcid.org/0000-0003-3349-8389; Email: cristian.ciraci@iit.it

### Authors

**Gonzalo Álvarez-Pérez** − *Istituto Italiano di Tecnologia, Center for Biomolecular Nanotechnologies, 73010 Arnesano, Italy;* orcid.org/0000-0002-4633-1898

**Tadele Orbula Otomalo** − *Istituto Italiano di Tecnologia, Center for Biomolecular Nanotechnologies, 73010 Arnesano, Italy;* orcid.org/0000-0002-2716-502X

Complete contact information is available at: https://pubs.acs.org/10.1021/acsphotonics.4c01308



### Funding

This work was supported by funding from the European Innovation Council through its Horizon Europe program with Grant Agreement No. 101046329.

### Notes

The authors declare no competing financial interest.


## REFERENCES


(1) Boyd, R. W. *Nonlinear Optics.*, 3rd ed.; Academic Press, Inc.: USA, 2008.

(2) Krasavin, A. V.; Ginzburg, P.; Zayats, A. V. Free-electron optical nonlinearities in plasmonic nanostructures: a review of the hydrodynamic description. *Laser Photonics Rev.* **2018**, *12*, No. 1700082.

(3) Almeida, V. R.; Lipson, M. Optical bistability on a silicon chip. *Opt. Lett.* **2004**, *29*, 2387−2389.

(4) Gibbs, H.; Tarng, S.; Jewell, J.; Weinberger, D.; Tai, K.; Gossard, A.; McCall, S.; Passner, A.; Wiegmann, W. Room-temperature excitonic optical bistability in a GaAs-GaAlAs superlattice étalon. *Appl. Phys. Lett.* **1982**, *41*, 221−222.

(5) Un, I.-W.; Sarkar, S.; Sivan, Y. Electronic-based model of the optical nonlinearity of low-electron-density Drude materials. *Phys. Rev. Appl.* **2023**, *19*, No. 044043.

(6) Cox, J. D.; García, J.; de Abajo, F. Electrically tunable nonlinear plasmonics in graphene nanoislands. *Nat. Commun.* **2014**, *5*, 5725.

(7) Christensen, T.; Yan, W.; Jauho, A.-P.; Wubs, M.; Mortensen, N. A. Kerr nonlinearity and plasmonic bistability in graphene nanoribbons. *Phys. Rev. B* **2015**, *92*, No. 121407.

(8) Cox, J. D.; Silveiro, I.; García de Abajo, F. J. Quantum effects in the nonlinear response of graphene plasmons. *ACS Nano* **2016**, *10*, 1995−2003.

(9) Ryabov, D.; Pashina, O.; Zograf, G.; Makarov, S.; Petrov, M. Nonlinear optical heating of all-dielectric super-cavity: efficient light-to-heat conversion through giant thermorefractive bistability. *Nanophotonics* **2022**, *11*, 3981−3991.

(10) Niu, J.; Shao, H.; Feng, Y.; Gao, B.; Zhang, Y.; Li, Y.; Chen, H.; Qian, H. All-Optical Nonlinear Neuron Based on Metallic Quantum Wells. *Adv. Opt. Mater.* **2023**, *11*, No. 2300223.
(11) Lee, J.; Tymchenko, M.; Argyropoulos, C.; Chen, P.-Y.; Lu, F.; Demmerle, F.; Boehm, G.; Amann, M.-C.; Alu, A.; Belkin, M. A. Giant nonlinear response from plasmonic metasurfaces coupled to intersubband transitions. *Nature* **2014**, *511*, 65−69.
(12) Taliercio, T.; Biagioni, P. Semiconductor infrared plasmonics. *Nanophotonics* **2019**, *8*, 949−990.
(13) Scalora, M.; Vincenti, M. A.; de Ceglia, D.; Roppo, V.; Centini, M.; Akozbek, N.; Bloemer, M. Second-and third-harmonic generation in metal-based structures. *Phys. Rev. A* **2010**, *82*, No. 043828.
(14) Ciracì, C.; Poutrina, E.; Scalora, M.; Smith, D. R. Second-harmonic generation in metallic nanoparticles: Clarification of the role of the surface. *Phys. Rev. B* **2012**, *86*, No. 115451.
(15) Khalid, M.; Ciracì, C. Enhancing second-harmonic generation with electron spill-out at metallic surfaces. *Commun. Phys.* **2020**, *3*, 214.
(16) De Luca, F.; Ortolani, M.; Ciracì, C. Free electron nonlinearities in heavily doped semiconductors plasmonics. *Phys. Rev. B* **2021**, *103*, No. 115305.
(17) De Luca, F.; Ciracì, C. Impact of surface charge depletion on the free electron nonlinear response of heavily doped semiconductors. *Phys. Rev. Lett.* **2022**, *129*, No. 123902.
(18) De Luca, F.; Ortolani, M.; Ciracì, C. Free electron harmonic generation in heavily doped semiconductors: the role of the materials properties. *EPJ. Appl. Metamat.* **2022**, *9*, 13.
(19) Rossetti, A. et al. Origin of optical nonlinearity in plasmonic semiconductor nanostructures. *arXiv preprint* **2024**, arXiv:2402.15443, https://arxiv.org/abs/2402.15443 (accessed Feb 23, 2024).
(20) Ruppin, R. Optical properties of a plasma sphere. *Phys. Rev. Lett.* **1973**, *31*, 1434.
(21) Ruppin, R. Extinction properties of thin metallic nanowires. *Opt. Commun.* **2001**, *190*, 205−209.
(22) Raza, S.; Toscano, G.; Jauho, A.-P.; Wubs, M.; Mortensen, N. A. Unusual resonances in nanoplasmonic structures due to nonlocal response. *Phys. Rev. B* **2011**, *84*, No. 121412.
(23) Benisty, H.; Greffet, J.-J.; Lalanne, P. *Introduction to nanophotonics*; Oxford university press, 2022.
(24) Anderegg, M.; Feuerbacher, B.; Fitton, B. Optically excited longitudinal plasmons in potassium. *Phys. Rev. Lett.* **1971**, *27*, 1565.
(25) Lindau, I.; Nilsson, P. Experimental verification of optically excited longitudinal plasmons. *Phys. Scr.* **1971**, *3*, 87.
(26) De Ceglia, D.; Scalora, M.; Vincenti, M. A.; Campione, S.; Kelley, K.; Runnerstrom, E. L.; Maria, J.-P.; Keeler, G. A.; Luk, T. S. Viscoelastic optical nonlocality of low-loss epsilon-near-zero nanofilms. *Sci. Rep.* **2018**, *8*, 9335.
(27) Christensen, T.; Yan, W.; Raza, S.; Jauho, A.-P.; Mortensen, N. A.; Wubs, M. Nonlocal response of metallic nanospheres probed by light, electrons, and atoms. *ACS Nano* **2014**, *8*, 1745−1758.
(28) Ciracì, C.; Della Sala, F. Quantum hydrodynamic theory for plasmonics: Impact of the electron density tail. *Phys. Rev. B* **2016**, *93*, No. 205405.
(29) Toscano, G.; Straubel, J.; Kwiatkowski, A.; Rockstuhl, C.; Evers, F.; Xu, H.; Asger Mortensen, N.; Wubs, M. Resonance shifts and spill-out effects in self-consistent hydrodynamic nanoplasmonics. *Nat. Commun.* **2015**, *6*, 7132.
(30) Ciracì, C. Current-dependent potential for nonlocal absorption in quantum hydrodynamic theory. *Phys. Rev. B* **2017**, *95*, No. 245434.
(31) Silberberg, Y.; Sands, T. Optical properties of metallic quantum wells. *IEEE J. Quantum Electron.* **1992**, *28*, 1663−1669.
(32) Qian, H.; Xiao, Y.; Liu, Z. Giant Kerr response of ultrathin gold films from quantum size effect. *Nat. Commun.* **2016**, *7*, No. 13153.
(33) Qian, H.; Li, S.; Chen, C.-F.; Hsu, S.-W.; Bopp, S. E.; Ma, Q.; Tao, A. R.; Liu, Z. Large optical nonlinearity enabled by coupled metallic quantum wells. *Light Sci. Appl.* **2019**, *8*, 13.
(34) Pirotta, S.; Tran, N.-L.; Jollivet, A.; Biasiol, G.; Crozat, P.; Manceau, J.-M.; Bousseksou, A.; Colombelli, R. Fast amplitude modulation up to 1.5 GHz of mid-IR free-space beams at room-temperature. *Nat. Commun.* **2021**, *12*, 799.
(35) Malerba, M.; Pirotta, S.; Aubin, G.; Lucia, L.; Jeannin, M.; Manceau, J.-M.; Bousseksou, A.; Lin, Q.; Lampin, J.-F.; Peytavit, E.; Barbieri, S.; Li, L.; Davies, G.; Linfield, E. H.; Colombelli, R. Ultrafast (≈ 10 GHz) mid-IR modulator based on ultrafast electrical switching of the light−matter coupling. *Appl. Phys. Lett.* **2024**, *125*, No. 041101.
(36) Jeannin, M.; Cosentino, E.; Pirotta, S.; Malerba, M.; Biasiol, G.; Manceau, J.-M.; Colombelli, R. Low intensity saturation of an ISB transition by a mid-IR quantum cascade laser. *Appl. Phys. Lett.* **2023**, *122*, 241107.
(37) Zanotto, S.; Mezzapesa, F. P.; Bianco, F.; Biasiol, G.; Baldacci, L.; Vitiello, M. S.; Sorba, L.; Colombelli, R.; Tredicucci, A. Perfect energy-feeding into strongly coupled systems and interferometric control of polariton absorption. *Nat. Phys.* **2014**, *10*, 830−834.
(38) Jeannin, M.; Manceau, J.-M.; Colombelli, R. Unified description of saturation and bistability of intersubband transitions in the weak and strong light-matter coupling regimes. *Phys. Rev. Lett.* **2021**, *127*, No. 187401.
(39) Cominotti, R.; Leymann, H.; Nespolo, J.; Manceau, J.-M.; Jeannin, M.; Colombelli, R.; Carusotto, I. Theory of coherent optical nonlinearities of intersubband transitions in semiconductor quantum wells. *Phys. Rev. B* **2023**, *107*, No. 115431.
(40) Baumberg, J. J.; Aizpurua, J.; Mikkelsen, M. H.; Smith, D. R. Extreme nanophotonics from ultrathin metallic gaps. *Nat. Mater.* **2019**, *18*, 668−678.
(41) Johnson, P. B.; Christy, R.-W. Optical constants of the noble metals. *Phys. Rev. B* **1972**, *6*, 4370.
(42) Moreau, A.; Ciracì, C.; Mock, J. J.; Hill, R. T.; Wang, Q.; Wiley, B. J.; Chilkoti, A.; Smith, D. R. Controlled-reflectance surfaces with film-coupled colloidal nanoantennas. *Nature* **2012**, *492*, 86−89.
(43) Hu, H.; Shi, Z.; Zhang, S.; Xu, H. Unified treatment of scattering, absorption, and luminescence spectra from a plasmon−exciton hybrid by temporal coupled-mode theory. *J. Chem. Phys.* **2021**, *155*, No. 074104.
(44) Silvestri, M.; Sahoo, A.; Assogna, L.; Benassi, P.; Ferrante, C.; Ciattoni, A.; Marini, A. Resonant third-harmonic generation driven by out-of-equilibrium electron dynamics in sodium-based near-zero index thin films. *Nanophotonics* **2024**, *13*, 2003−2013.
(45) Huang, Z.; Baron, A.; Larouche, S.; Argyropoulos, C.; Smith, D. R. Optical bistability with film-coupled metasurfaces. *Opt. Lett.* **2015**, *40*, 5638−5641.
(46) Argyropoulos, C.; Chen, P.-Y.; D'Aguanno, G.; Engheta, N.; Alu, A. Boosting optical nonlinearities in ε-near-zero plasmonic channels. *Phys. Rev. B* **2012**, *85*, No. 045129.
(47) Hu, H.; Álvarez-Pérez, G.; Otomalo, T. O.; Ciracì, C. Low-power threshold optical bistability enabled by hydrodynamic Kerr nonlinearity of free-carriers in heavily doped semiconductors. *arXiv preprint* **2024**, arXiv:2406.07750, https://arxiv.org/abs/2406.07750 (accessed Jun 11, 2024).


https://doi.org/10.1021/acsphotonics.4c01308
*ACS Photonics* 2024, 11, 4812−4817